

Ashik & Daud, 2016

Volume 2 Issue 1, pp.42-52

Year of Publication: 2016

DOI- <http://dx.doi.org/10.20319/mijst.2016.21.4252>

This paper can be cited as: Ashik, U., & Daud, W. W. (2016). Stability Enhancement of Nano-NiO Catalyst with SiO₂ Support to get Improved Hydrogen Yield from Methane Decomposition. *MATTER: International Journal of Science and Technology*, 2(1), 42-52.

This work is licensed under the Creative Commons Attribution-Non Commercial 4.0 International License. To view a copy of this license, visit <http://creativecommons.org/licenses/by-nc/4.0/> or send a letter to Creative Commons, PO Box 1866, Mountain View, CA 94042, USA.

STABILITY ENHANCEMENT OF NANO-NiO CATALYST WITH SiO₂ SUPPORT TO GET IMPROVED HYDROGEN YIELD FROM METHANE DECOMPOSITION

U.P.M. Ashik

Department of Chemical Engineering, University of Malaya, 50603, Kuala Lumpur, Malaysia

W.M.A. Wan Daud

Department of Chemical Engineering, University of Malaya, 50603, Kuala Lumpur, Malaysia

Abstract

Building of the nanoparticle from their precursors by bottom-up method is a very fascinating practice in nanotechnology. Most promising two bottom-up methods are experimentally unveiled in this research contribution; i) controlled precipitation of Ni nanoparticles and their reinforcement with silicate by modified Stöber method and ii) chemical vapor deposition of nano-carbon from methane over silicate supported nano-Ni catalyst. We found that the silicate addition results in the formation of single crystal NiO nanoparticles which exhibited catalytic activity enhancing features, such as low particle size and high surface area and porosity. The single-point surface area was increased from 62.22 m²/g to 91.50 m²/g for n-Ni O nanoparticles, after silicate incorporation. Preliminary catalytic activity was also analyzed in a fixed-bed pilot plant. N-NiO/SiO₂ nanoparticles generated 57.28% hydrogen at 730 °C. Isothermal methane decomposition was conducted at 625 °C to examine the stability of catalyst.

Keywords

Nano-catalysts; Modified Stöber method; Thermo catalytic Methane decomposition; Hydrogen;
Nano-carbon; Bottom-up method

1. Introduction

Nanotechnology has wide application in almost any scientific field. The ubiquitous possibilities of using nanotechnology are mainly due to the property enhancement that occurs in nanoparticles at their unique size and shape. Research on nanotechnology primarily focuses on developing novel nanoparticles with small size and refined shapes. The synthesis of fine nanoparticles demands a well knowledge of the surface characteristics of these materials. The quality and structure of nanoparticles play a vital role in their potential applications. Nanoparticles can be synthesized using two methods: bottom-up and top-down. The bottom-up approach is a technique in which nanoparticles are built from the bottom through atom-by-atom, molecule-by-molecule, or cluster-by-cluster. This well-established method ensures the formation of nanoparticles with less defects, homogeneous chemical composition, and improved crystal ordering (Castelino, Satyanarayana, & Sitti, 2005; Lu & Lieber, 2007). By contrast, the top-down method is rarely applied to convert giant sized to man-sized particles because the physical stress applies during top-down approach generates surface defects and contaminants (Chan & Kwok, 2011).

In this study, *n*-Ni O nanoparticles were prepared through co-precipitation by using their respective metal nitrate solution. The as-prepared nanometer oxides were stabilized with silicate through modified Stöber method. Improvements in characteristics and activity were examined on metal oxide nanoparticles upon silicate reinforcement. Furthermore, the preliminary catalytic performance and isothermal catalytic activity of the synthesized catalysts at 625 °C was analyzed in a fixed-bed pilot plant.

2. Experimental section

2.1 Preparation of *n*-Ni O nano-particles and stabilization with SiO₂

Nanosized nickel hydroxide suspension was prepared through co-precipitation by treating nickel (II) nitrate hex hydrate (Across Organics) solution with ammonia (U. P. M. Ashik & Wan Mohd Ashri Wan Daud, 2015; Stöber, Fink, & Bohn, 1968). First, 0.02 mole nickel (II) nitrate

hex hydrate was homogeneously dissolved in 200 m L of water through sanitation. Metal hydroxide was precipitated by drop-wise addition of 6 m L of 30% NH_3 solution under sanitation for 1 h. The resulting suspension was stirred for another 1 h with a magnetic stirrer at room temperature. The precipitated metal hydroxide was acquired by centrifugation at 4000 rpm for 30 min. The precipitate was thoroughly washed with distilled water and ethanol and then dispersed in 100 m L of ethanol and continuously stirred for 15 h with magnet. The metal hydroxide precipitate was collected through centrifugation and dried at 100 °C for 15 h under air circulation. The dried sample was claimed at 350 °C for 3 h to convert metal hydroxides into metal oxides. The produced samples were named as *n*-Ni O.

The Ni (OH) ₂ dispersion in ethanol was prepared as described above and 4 m L of 8M NH_3 solution was added to the dispersion. Afterward, 0.4 m L of TEOS (Aldrich) and 0.4 m L of C18TMS (Acros Organics) were simultaneously added to the dispersion while soliciting. Sanitation was further continued for 1 h, and the reaction mixture was stirred with magnet for another 5 h. The precipitate was separated through centrifugation and dried in an oven at 100 °C for 15 h under air circulation. The dried product was claimed at 450 °C for 3 h to produce metal oxide/silica nanostructures by removing all organic moieties. The produced sample was named as *n*-Ni O/SiO₂.

2.2 Characterization techniques

Surface characteristics, such as pore size distribution, pore volume and surface area were evaluated by nitrogen adsorption–desorption measurements using Micromeritics ASAP 2020 BET apparatus at –196 °C. Transmission electron microscopy (TEM) images of fresh catalyst and produced halocarbon were acquired using FEI Tecnai™ instrument. N-Ni O and *n*-Ni O/SiO₂ nanoparticles were examined using PAN lyrical diffract meter. Average crystallite size was obtained using the global Scherer equation as follows:

$$D = \frac{K \lambda}{\beta \cos \theta}$$

where the crystallite size, peak length, line broadening full width at half-maxima after subtracting the instrumental line broadening (in radians), and the Bragg's angle are expressed as *D* (nm), λ (1.54056 Å), β , and 2θ , respectively. The Scherer constant is 0.9.

2.2 Preliminary catalytic activity analysis

A fixed catalyst bed pilot plant constructed with stainless steel (SS310S) was used for conducting methane decomposition catalytic activity examination. The experimental apparatus used for production of greenhouse gas (GHG) free hydrogen from methane is described in detail elsewhere (U. P. M. Ashik & Wan Mohd Ashri Wan Daud, 2015; U. P. M. Ashik & W. M. A. Wan Daud, 2015). About 1 g of the catalyst was homogeneously distributed over the catalyst bed for preliminary temperature programmed methane decomposition (TPD). The catalyst was reduced at 550 °C with 30% H₂ balanced with N₂ for 2.5 h. After completing the reduction stage, TPD was conducted with decomposition from 200 °C to 900 °C with a ramp of 5 °C/min. The mole percentage of gas component in the out stream gas was calculated using the online analyzer Rosemount Analytical X-STREAM (UK).

3. Results and discussion

3.1 XRD analysis

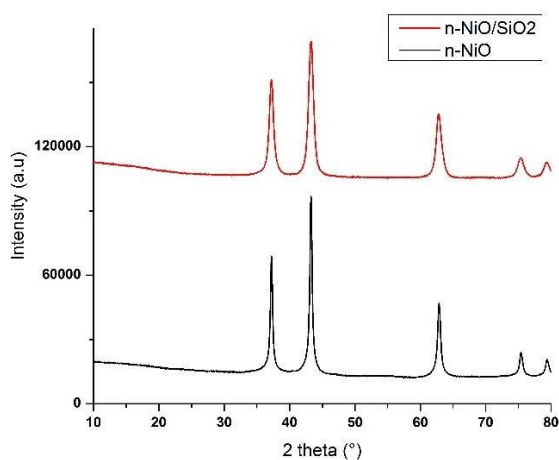


Figure 1: XRD patterns of *n*-Ni O and *n*-Ni O /SiO₂.

Figure. 1 shows the XRD patterns of the claimed *n*-Ni O and *n*-Ni O/SiO₂. The crystalline size and plane that correspond to each peak according to the Scherrer equation are provided in Table 1. The crystallite size calculated from XRD approve the mean particle size obtained from N₂ adsorption–desorption analysis, as exhibited in Table 2. The catalyst performance and its longevity are strongly influenced by the degree of structural order. The XRD patterns for *n*-Ni O and *n*-Ni O/SiO₂ [Figure. 1] exhibit three major diffraction peaks, which correspond to (111),

(200), and (220) solid reflections. The diffraction peaks for *n*-Ni O centered at $2\theta = 37.20^\circ$, 43.47° , 62.75° , 75.43° , and 79.39° with corresponding *d*-spacing values of 2.414, 2.079, 1.479, 1.259, and 1.205 Å, respectively. The *n*-Ni O diffraction peaks are in good agreement with those given in JCPDS No. 00-047-1049 for cubic Ni O phase. On the contrary, the diffraction peaks of *n*-Ni O slightly varied after the addition of silicate, and the revised peaks are in good agreement with cubic Ni O (JCPDS No. 01-073-1523). It is obvious from the XRD patterns that the peaks for silicate-supported Ni O are broader than that of pure *n*-Ni O peaks, indicating its smaller crystalline size after being supported with SiO₂. These results are clearly supported by the BET mean particle sizes shown in Table 2. The absence of specific peaks for silicate may be attributed to its amorphous characteristics.

Table 1: Major crystal planes and their corresponding crystallite sizes of all prepared nanoparticles from XRD analysis

Sample	Plane/(nm)	Plane/(nm)	Plane/(nm)	Avg. (nm)
<i>n</i> -Ni O	(111)/30.91	(200)/32.89	(220)/39.46	34.42
<i>n</i> -Ni O /SiO ₂	(111)/33.25	(200)/31.74	(220)/31.19	32.06

Porosity analysis

Porosity analysis on the exposed surfaces of the prepared nanoparticles was conducted using N₂ adsorption–desorption measurements. *N*-Ni O, *n*-Ni O/SiO₂ exhibited type IV N₂ adsorption–desorption isotherms (not shown in article) revealed their mesoporous characteristics. However, the beginning portion of the isotherms analogous to type I isotherm attributed to the presence of small amounts of microspores in the materials. The single-point surface area, BET surface area, pore volume, average pore size, and average particle size of the produced nanocatalysts are also presented in Table 2. The single-point surface area, BET surface area, and mesoporous area were marginally increased after silicate addition. The single-point surface area of *n*-Ni O increased from 62.22 m²/g to 91.50 m²/g after being supported with silicate. Furthermore, the BET particle size of the unsupported *n*-Ni O (48.02 nm) marginally decreased to 32.19 nm after the incorporation of the silicate support. This shrinkage of particle size is attributed to the protection of metal oxide particles from agglomeration during high-temperature calcinations.

Table 2: Physical characteristics of *n*-Ni O, *n*-Ni O/SiO₂, *n*-Fe O, *n*-Fe O/SiO₂, *n*-Co O and *n*-Co O/SiO₂ from N₂ adsorption-desorption analysis.

Catalyst	Single point S A ^a (m ² /g)	BET SA (m ² /g)	Micropore area ^b (m ² /g)	Mesopore + external area ^c (m ² /g)	Micropore volume (cm ³ /g)	Mesoporous volume (cm ³ /g)	Total pore volume (cm ³ /g)	BET pore size (nm)	Mean particle size (nm)
<i>n</i> -Ni O	62.22	62.46	5.17	57.28	0.0020	0.2479	0.2499	16.274	48.02
<i>n</i> -Ni O/SiO ₂	91.50	93.18	5.17	88.01	0.0024	0.2277	0.2301	9.987	32.19

^a Represents the values calculated at a relative pressure (P/P₀) of N₂ equal to 0.301.

^{b-d} represents the values calculated from *t*-plot method.

^c Represents the total pore volume evaluated from nitrogen uptake at a relative pressure (P/P₀) of N₂ equal to 0.98.

3.2 Morphology analysis

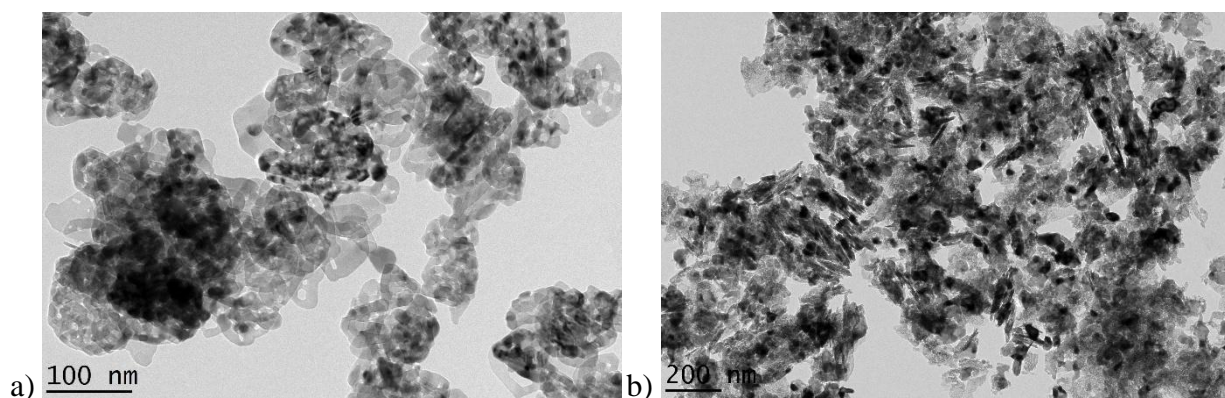


Figure 2: TEM images of a) *n*-Ni O and b) *n*-Ni O/SiO₂.

TEM images of the produced *n*-Ni O and *n*-Ni O/SiO₂ are shown in Figs. 2 (a and b), respectively. Produced nanoparticles were formed with uniform size distribution. However, they exhibited different shaped in TEM images. Electron transmission investigation showed large particles with smooth external surfaces and edges for *n*- Ni O before being supported with SiO₂ [Figs. 2 (a)]. After supporting with silicate, the *n*-Ni O particles exhibited relatively rough morphology with smaller size [Figs. 2 (b)]. Decrease in size observed with particles is in good agreement with the BET (Table 2) and XRD (Fig. 1 and Table 1) results.

3.3 Temperature programmed methane decomposition

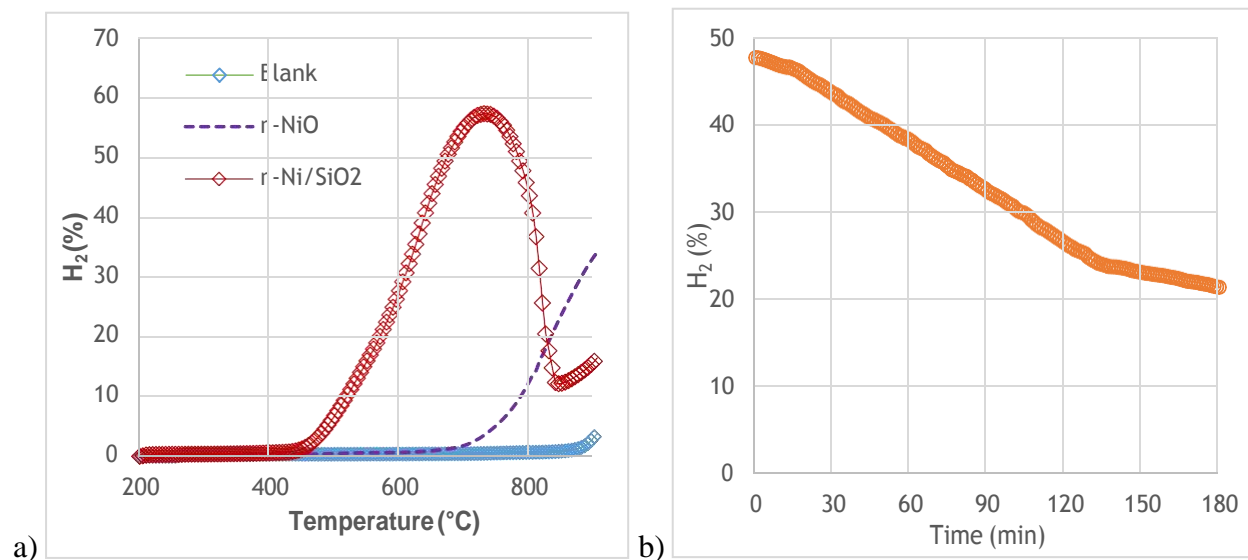


Figure 3: Production of hydrogen (in percentage) during temperature programmed methane decomposition over 1g of *n*-Ni O and *n*-Ni O/SiO₂ catalysts. b) Isothermal methane decomposition over *n*-Ni O/SiO₂ catalyst at 625 °C.

The catalytically active temperature a zone of naked and supported nickel catalyst was examined by temperature programmed methane decomposition (TPD), and the results are displayed in Fig. 3. Hydrogen formation was observed after 880 °C in the absence of catalyst. However, in the presence of *n*-Ni O catalyst, methane was started to decompose in to hydrogen and halocarbon at 700 °C. Methane conversion was increased with increasing temperature, supporting the exothermic behavior of methane decomposition (Ashik, Wan Daud, & Abbas, 2015). The silicate support created huge changes on the catalyst activity of *n*-Ni O. Irrespective of the activity zone of *n*-Ni O, *n*-Ni O/SiO₂ nanoparticles exhibited a remarkable catalytically active zone between 450 °C and 730 °C, with a maximum hydrogen production of 57.28% at 730 °C. *n*-NiO/SiO₂ started to deactivate above 730 °C, and hydrogen production decreased to 12% at 845 °C and then started to gradually increase according to the endothermic nature of methane decomposition. Thermal degradation occurred at higher temperature may be a reason of deactivation of *n*-Ni O/SiO₂ after achieving the maximum hydrogen production percentage (Lee, Yeoh, Chai, Ichikawa, & Mohamed, 2012). The experimented *n*-Ni O/SiO₂ catalyst is superior to the naked and supported metal catalysts prepared using conventional methods at 500 °C to 700

°C (Ashok, Reddy, Raju, Subrahmanyam, & Venugopal, 2009; Figueiredo, Órfão, & Cunha, 2010; Nuernberg et al., 2012). This finding clearly shows the advantages of co-precipitation cum modified sober method.

The stability of $n\text{-Ni O/SiO}_2$ was examined by conducting isothermal methane decomposition at 625 °C for 180 minutes [Fig. 3 (b)]. The catalyst exhibited an initial hydrogen production of 48% and slightly decreased with time. The final hydrogen production after 180 minutes of isothermal examination was 21.3%, which indicates the presence of active Ni-phases even after a long span carbon deposition. It may be attributed to the formation of carbon monofilaments with Ni particles at their tip as shown in TEM image [Fig. 5 (b)].

3.4 Characterization of produced halocarbon

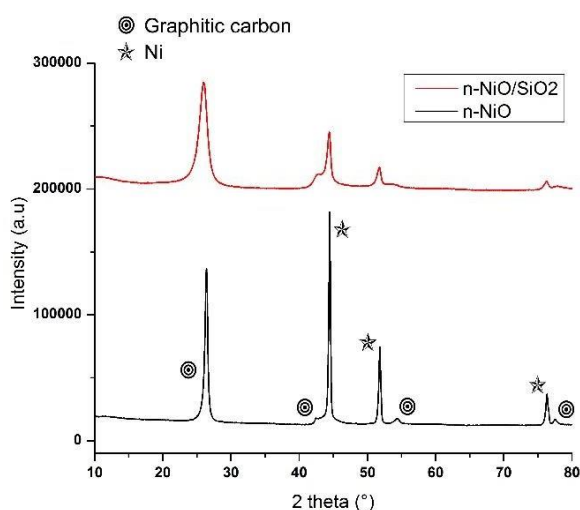


Figure 4: XRD patterns of $n\text{-Ni O}$ and $n\text{-Ni O/SiO}_2\text{TPD}$. Peaks correspond to graphitic carbon and Ni is indicated.

The presence of graphitic carbon can be easily identified by the XRD patterns of $n\text{-Ni O}$ and $n\text{-Ni O/SiO}_2$ after TPD (Fig. 4). The as-obtained carbon over Ni-based catalysts can be distinguished by diffraction peaks observed at $2\theta = 26.44^\circ$, 42.49° , 44.47° , 54.48° , and 76.34° in Fig. 4 (a), which are in good agreement with JCPDS No. 00-001-0640 for hexagonal graphitic carbon. Furthermore, the diffraction peaks for completely reduced Ni can be seen at $2\theta = 44.47^\circ$, 51.83° , and 76.34° , indicating the reduction capability of methane. The diffraction peaks for Ni

observed over n -Ni O and n -Ni O/SiO₂ after temperature-programmed methane decomposition are similar to the peaks in JCPDS No. 01-070-1849 for cubic metallic Ni.

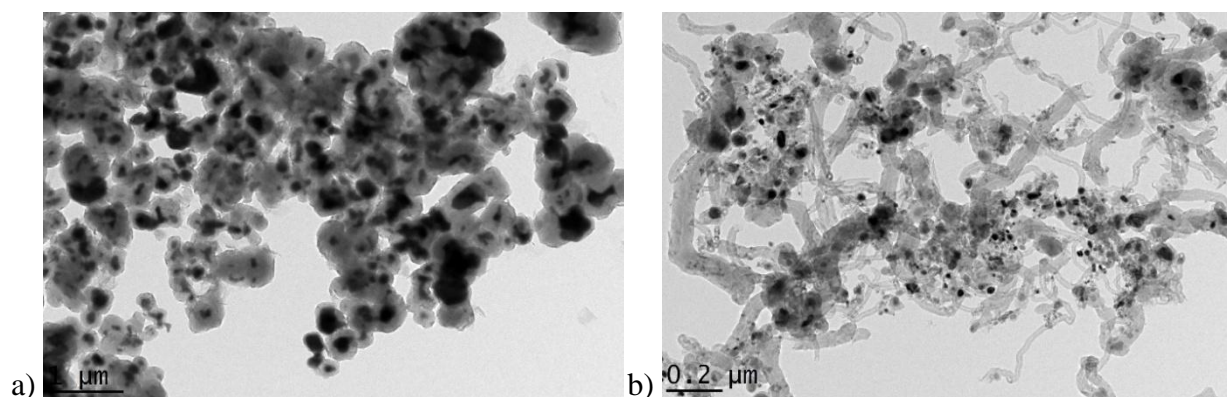


Figure 5: TEM images of a) n -Ni O and b) n -Ni O/SiO₂ nano-catalysts after TPD.

The TEM images of n -Ni O and n -Ni O/SiO₂ after TPD are shown in Fig. 5. The unsupported n -Ni O particles underwent fast agglomeration resulted in the formation of large particles, and were completely encapsulated by the as-produced halocarbon [Figs. 5 (a)]. The carbon covered and isolates metal particles from the reaction medium and prevented further methane decomposition (Kim, Rodriguez, & Baker, 1991). However, silicate-supported n -NiO effectively prevented particle agglomeration and allowed advanced methane decomposition, resulting in the production of nanocarbon filaments [Figs. 5 (b)].

4. Conclusion

Modified Stöber method was adopted to stabilize metal oxide nanoparticles at room temperature without using any surface-coupling agent. Characteristic investigations demonstrated that the catalytic characteristics of nanometer oxides were enhanced after being supported with silicate. The particle sizes of n -Ni O marginally decreased from 48.02 nm to 32.19, nm. Further surface and porous features, crystallite sizes, and reduction characteristics were enhanced accordingly. n -Ni O/SiO₂ catalysts showed an outstanding performance between 450 °C and 730 °C with a maximum hydrogen production value of 57.28%. n -Ni O/SiO₂ exhibited better stability at 625 °C without undergoing much deactivation.

5. Acknowledgment

The authors gratefully acknowledge financial support from the postgraduate Research Fund (UM.C/HIR/MOHE/ENG/11), University of Malaya, Malaysia.

REFERENCES

- Ashik, U. P. M., & Daud, W. M. A. W. (2015). Nano-nickel catalyst reinforced with silicate for methane decomposition to produce hydrogen and nanocarbon: synthesis by co-precipitation cum modified Stober method. *RSC Advances*, 5, 46735-46748. doi:10.1039/C5RA07098H <http://dx.doi.org/10.1039/C5RA07098H>
- Ashik, U. P. M., & Daud, W. M. A. W. (2015). Probing the differential methane decomposition behaviors of n-Ni/SiO₂, n-Fe/SiO₂ and n-Co/SiO₂ catalysts prepared by co-precipitation cum modified Stober method. *RSC Advances*, 5(82), 67227-67241. doi:10.1039/C5RA10997C <http://dx.doi.org/10.1039/C5RA10997C>
- Ashik, U. P. M., Wan Daud, W. M. A., & Abbas, H. F. (2015). Production of greenhouse gas free hydrogen by thermocatalytic decomposition of methane – A review. *Renewable and Sustainable Energy Reviews*, 44(0), 221-256. doi:http://dx.doi.org/10.1016/j.rser.2014.12.025 <http://dx.doi.org/10.1016/j.rser.2014.12.025>
- Ashok, J., Reddy, P. S., Raju, G., Subrahmanyam, M., & Venugopal, A. (2009). Catalytic Decomposition of Methane to Hydrogen and Carbon Nanofibers over Ni–Cu–SiO₂ Catalysts. *Energy & Fuels*, 23(1), 5-13. doi:10.1021/ef8003976 <http://dx.doi.org/10.1021/ef8003976>
- Castelino, K., Satyanarayana, S., & Sitti, M. (2005). Manufacturing of two and three-dimensional micro/nanostructures by integrating optical tweezers with chemical assembly. *Robotica*, 23(04), 435-439. doi:doi:10.1017/S0263574704000864
- Chan, H.-K., & Kwok, P. C. L. (2011). Production methods for nanodrug particles using the bottom-up approach. *Advanced Drug Delivery Reviews*, 63(6), 406-416. doi:http://dx.doi.org/10.1016/j.addr.2011.03.011 <http://dx.doi.org/10.1016/j.addr.2011.03.011>
- Figueiredo, J. L., Órfão, J. J. M., & Cunha, A. F. (2010). Hydrogen production via methane decomposition on Raney-type catalysts. *International Journal of Hydrogen Energy*,

- 35(18), 9795-9800. doi:<http://dx.doi.org/10.1016/j.ijhydene.2009.12.071> <http://dx.doi.org/10.1016/j.ijhydene.2009.12.071>
- Kim, M. S., Rodriguez, N. M., & Baker, R. T. K. (1991). The interaction of hydrocarbons with copper-nickel and nickel in the formation of carbon filaments. *Journal of Catalysis*, 131(1), 60-73. doi:[http://dx.doi.org/10.1016/0021-9517\(91\)90323-V](http://dx.doi.org/10.1016/0021-9517(91)90323-V) [http://dx.doi.org/10.1016/0021-9517\(91\)90323-V](http://dx.doi.org/10.1016/0021-9517(91)90323-V)
- Lee, K.-Y., Yeoh, W.-M., Chai, S.-P., Ichikawa, S., & Mohamed, A. R. (2012). Catalytic Decomposition of Methane to Carbon Nanotubes and Hydrogen: The Effect of Metal Loading on the Activity of CoO-MoO/Al₂O₃ Catalyst. *Fullerenes, Nanotubes and Carbon Nanostructures*, 21(2), 158-170. doi:10.1080/1536383X.2011.597007 <http://dx.doi.org/10.1080/1536383X.2011.597007>
- Lu, W., & Lieber, C. M. (2007). Nanoelectronics from the bottom up. *Nat Mater*, 6(11), 841-850. Retrieved from <http://dx.doi.org/10.1038/nmat2028> <http://dx.doi.org/10.1038/nmat2028>
- Nuernberg, G. D. B., Foletto, E. L., Campos, C. E. M., Fajardo, H. V., Carreño, N. L. V., & Probst, L. F. D. (2012). Direct decomposition of methane over Ni catalyst supported in magnesium aluminate. *Journal of Power Sources*, 208(0), 409-414. doi:<http://dx.doi.org/10.1016/j.jpowsour.2012.02.037> <http://dx.doi.org/10.1016/j.jpowsour.2012.02.037>
- Stöber, W., Fink, A., & Bohn, E. (1968). Controlled growth of monodisperse silica spheres in the micron size range. *Journal of Colloid and Interface Science*, 26(1), 62-69. doi:[http://dx.doi.org/10.1016/0021-9797\(68\)90272-5](http://dx.doi.org/10.1016/0021-9797(68)90272-5) [http://dx.doi.org/10.1016/0021-9797\(68\)90272-5](http://dx.doi.org/10.1016/0021-9797(68)90272-5)